RSC Advances

PAPER

View Article Online
View Journal | View Issue



Cite this: *RSC Adv.*, 2025, **15**, 3849

# Selective arrangement of three types of calcium–terbium tetranuclear cores by a thiacalixarene ligand using thermodynamic and kinetic strategies†

Ryunosuke Karashimada, * Hironori Matsuoka and Nobuhiko Iki*

Received 21st November 2024
Accepted 17th January 2025

DOI: 10.1039/d4ra08259a

rsc.li/rsc-advances

In this study, we report thermodynamic and kinetic strategies for arranging three types of Ca–Tb heterotetranuclear cores in a square configuration sandwiched by thiacalix[4]arene-*p*-tetrasulfonate (TCAS) ligands in aqueous solutions. In the thermodynamic strategy, the components were mixed under optimum pH conditions to afford a complex with a desired ratio of Ca:Tb:TCAS. In the kinetic strategy, the $Ca_1Tb_3TCAS_2$ complex was formed *via* mixing kinetically stable $Tb_3TCAS_2$ with $Ca^{2+}$. Interestingly, the resulting complexes ($Ca_xTb_{4-x}TCAS_2$, $x = 1$–3) exhibited Tb-centered luminescence upon excitation of the TCAS center with a high quvdantum yield ($\phi$ = 0.11–0.14) and a long luminescence lifetime (approximately 1.2 ms). The thermodynamic strategy can be applied to $Sr^{2+}$ instead of $Ca^{2+}$, but it is not suitable for first transition metal ions. However, the kinetic strategy is versatile and can be applied to first transition metal ions to afford $M_1Tb_3TCAS_2$ (M = $Sr^{2+}$, $Mn^{2+}$, $Fe^{2+}$, $Co^{2+}$, $Ni^{2+}$, $Cu^{2+}$, $Zn^{2+}$).



## Introduction

The functionality of metal complexes arises from the ligand and the metal center. Introducing different metal centers to a complex to form a heteronuclear complex can result in novel functions imparted by metal–metal interactions and are of significant interest to chemists. Many heteronuclear complexes have been used as luminescent materials, magnetic materials (single molecule magnets), and catalysts.[1]

Lanthanide (Ln) complexes exhibit potential as bio-imaging materials, such as luminescence probes and contrast agents for magnetic resonance imaging (MRI).[2] To enhance the performance of Ln-based probes, the design of a heteronuclear complex featuring different metal centers (d–f or f–f metal centers) can be useful.[1a,3] The d–f and f–f heteronuclear complexes can provide multifunctionality and novel functions through interactions between the metal centers, such as dual luminescence, up-conversion, and multimodalities (*e.g.*, luminescence imaging and MRI).[4–7]

Thermodynamic and kinetic strategies (Fig. 1) are known approaches for the selective synthesis of a single heteronuclear complex.[3a] In the thermodynamic strategy, two coordination sites of a ligand are designed to provide selectivity towards two metal ions, enabling the binding of distinct metal centers. This thermodynamic strategy is straightforward to implement because of the simple mixing of the ligand and metal ions. Furthermore, the metal centers are in close proximity for their interactions. However, the chemical properties of the metal ions should be significantly different; consequently, the combination of metal ions is limited to d–d or d–f. In the f–f combination, obtaining site-selective coordination is impossible. Moreover, the resulting complex should be kinetically stable, otherwise the Ln and Ln′ ions in the formed complex shuffle between different coordination sites.

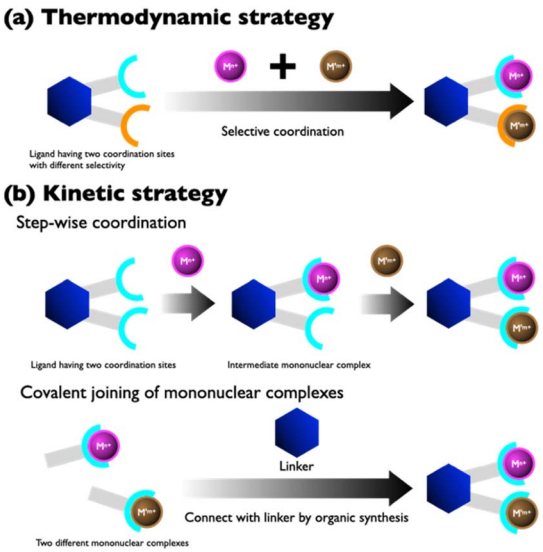


Fig. 1 Schematics of the (a) thermodynamic and (b) kinetic strategies for the selective synthesis of a heteronuclear complex.

*Graduate School of Environmental Studies, Tohoku University, 6-6-07, Aramaki-Aoba, Aoba-ku, Sendai 980-8579, Japan. E-mail: karashimada@tohoku.ac.jp; iki@tohoku.ac.jp*

† Electronic supplementary information (ESI) available. See DOI: https://doi.org/10.1039/d4ra08259a

Two methods are used to implement the kinetic strategy. The first method is the step-wise method, which involves the initial synthesis of a mononuclear complex. The mononuclear complex subsequently reacts with a different metal ion to form a heteronuclear complex. The other method is the covalent joining of two mononuclear complexes. These methods require kinetic stability of the mononuclear intermediates such that they do not release the metal center. Therefore, an *endo*-type ligand, such as 1,4,7,10-tetraazacyclododecane-1,4,7,10-tetraacetic acid (DOTA) is usually used as a coordination moiety (The definition of an *endo*-type ligand is one that can encapsulate a metal ion inside the ligand.[10b]). However, an *endo*-type ligand and linker moiety induce the opening of a large distance between the metal centers, which causes weakening of the f–f interaction due to wrapping of the metal centers by the *endo*-type ligand and separation by the linker moiety.

A coordination bond is dynamic, and its timescale significantly depends on the kinetic property of the metal center. Therefore, the kinetic stability of a heteronuclear complex is crucial in determining the formation of heteronuclear complexes. If a heteronuclear complex is kinetically unstable, the metal centers shuffle between the coordination sites, resulting in a decrease in the intended heteronuclear complex and the formation of unwanted homo- and heteronuclear complexes. Furthermore, the synthesis of a single heteronuclear complex is difficult due to the low selectivity of the coordination moiety of the ligand. This low selectivity of the coordination moiety can also result in the concomitant formation of unwanted homo- and heteronuclear complexes. Therefore, the development of selective synthesis methods and kinetically stable single heteronuclear complexes in aqueous solutions remains a significant challenge in research.

In a previous study, we reported that thiacalix[4]arene-*p*-tetrasulfonate (TCAS, Fig. 2) can be a ligand for complexes containing multiple Ln and M–Ln cores.[8] For example, Ln ions self-assemble to form a trinuclear Ln–TCAS complex ($Ln_3TCAS_2$, Fig. 2).[9] The TCAS ligand functions as an *exo*-type ligand, coordinating to the tri-Ln core through O,S,O donor sets located on the surface of TCAS. (The definition of an *exo*-type ligand is one that binds to a metal center at the surface of the ligand.[10b]). The $Ln_3TCAS_2$ complex exhibits Ln-centered luminescence (Ln = Tb, Yb, and Nd) through an energy-transfer mechanism with good luminescence properties, and possesses high proton relaxivity, and thus functions as a suitable contrast agent for MRI with kinetic stability.[9,10] Furthermore, d–f and f–f heteronuclear complexes, such as Ag–Ln–TCAS, Cd–Ln–TCAS, and Ln–Ln′–TCAS systems, have been successfully synthesized to attain distinctive functions that have not been achieved by mononuclear $Ln_1TCAS_1$.[7,11]

Simply mixing the components at pH 10 according to the thermodynamic strategy afforded $Ag_4Tb_1TCAS_2$, which showed an exceptionally long-lived Tb-centered luminescent lifetime (4.6 ms) in an aqueous solution by eliminating coordinated water molecules through the $O_8$-cubic coordination geometry provided by the two TCAS ligands.[11a,b] In another example, the Tb–Yb–TCAS system provided a mixture of homo- and heterotrinuclear complexes ($Tb_xYb_{3-x}TCAS_2$, $x$ = 0–3), in which heterotrinuclear complexes ($Tb_xYb_{3-x}TCAS_2$, $x$ = 1, 2) exhibited a Tb→Yb energy transfer, that is, f–f communication.[7] In contrast, following the kinetic strategy, the $Tb_1Yb_2TCAS_2$ complex can be selectively synthesized by isolating an intermediate complex ($Ln_1TCAS_1$, Fig. 2).[7] Thus, TCAS is a suitable ligand for the formation of d–f and f–f heteronuclear complexes.

In a recent experiment aimed at preparing $Tb_xYb_{3-x}TCAS_2$ ($x$ = 1, 2), we accidently found new heteronuclear complexes containing TCAS, $Ca^{2+}$, and $Tb^{3+}$ (Fig. 2) in the reaction mixture. The Ca–Tb–TCAS system modulates the stoichiometry of the Ca–Tb core by manipulating the Ca : Tb ratio and pH condition, which results in energy-transfer luminescence. Calcium ions play significant roles in cell membrane responses, serving as a biomaterial component, with applications for cancer therapy.[12]

In previous research on heteronuclear complexes,[4–6] a precise design and complicated synthesis of the ligands were required for the selective formation of heteronuclear complexes. For example, Piguet *et al.* reported some d-f heteronuclear complexes with a precisely designed ligand providing different coordination sites of 6 and 9 coordination numbers to d and f ions, respectively.[4] In contrast, our system only involves mixing the components (Ca, Tb, and TCAS) while controlling the pH condition for the formation of Ca–Tb–TCAS complexes without modification of the TCAS ligand.

In this study, we demonstrate the selective synthesis of three types of heterotetranuclear Ca–Tb–TCAS complexes using thermodynamic and kinetic strategies. Moreover, the study reveals the luminescent properties of the resulting complexes, and extending the strategies to metal ions other than $Ca^{2+}$ is also successfully demonstrated.

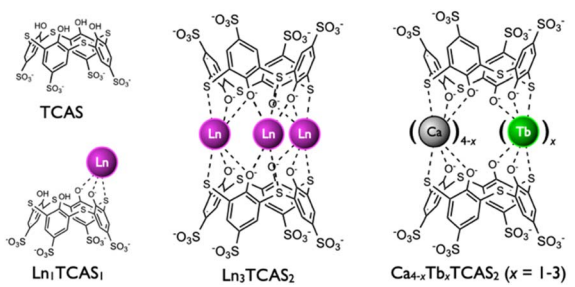


Fig. 2 Two-dimensional representations of TCAS, $Ln_1TCAS_1$, $Ln_3TCAS_2$, and heterotetranuclear Ca–Tb–TCAS complexes.

## Results and discussion

### Self-assembly of heterotetranuclear Ca–Tb–TCAS complexes using the thermodynamic strategy

In our previous study, we found an unknown trace in a reaction mixture used for selective synthesis of heterotrinuclear complexes ($Tb_xYb_{3-x}TCAS_2$, $x$ = 1, 2).[7b] It was confirmed that the unknown trace was a heteronuclear complex containing Tb $Tb^{3+}$, TCAS ($H_4tcas^{4-}$), and $Ca^{2+}$. Then, to synthesize Ca–Tb–TCAS complexes, the ratios of Ca:Tb:TCAS and pH conditions were varied. As a result, three types of heterotetranuclear Ca–

Tb–TCAS ($Ca_xTb_{4-x}TCAS_2$, $x = 1-3$) were selectively formed under the appropriate conditions, as confirmed by high-performance liquid chromatography (HPLC) peaks (peak 1, peak 2, and peak 3) with different retention times (Fig. 3). The HPLC conditions were 45 wt% $CH_3CN$ in $H_2O$ containing 10 mmol per kg HEPES (apparent pH 7.4) and 30 mmol per kg TBABr (HEPES = 2-[4-(2-hydroxyethyl)-1-pyperadinyl] ethanesulfonic acid, TBABr = tetrabutylammonium bromide).

Because previously reported $Ln_3TCAS_2$ complexes showed high kinetic stability under strongly acidic conditions (Ln = Yb: $t_{1/2} = 1.53$ h at pH 1.16 and Ln = Gd: $t_{1/2} = 2.4$ h at pH 2),[10a,b] it was expected that the heterotetranuclear Ca–Tb–TCAS complexes would exhibit high kinetic stability, implying that the dissociation reaction during the HPLC measurement is negligibly slow. The stoichiometry of the heterotetranuclear Ca–Tb–TCAS complexes was determined by employing the molar ratio method and electro-spray ionization-mass spectrometry (ESI-MS) analysis. Hereinafter, we describe the self-assembly of the ternary complex at the optimum pH (6.0, 10, and 11). In addition, conditions with different pH values resulted in a mixture of the complexes and/or TCAS ligand (as an example, at pH 7.4, as shown in Fig. S1†).

At pH 6.0, the molar ratio of $Tb^{3+}$/TCAS was fixed at 1.5, and the concentration of $Ca^{2+}$ was varied to investigate the height of peak 1 (Fig. 4). In zero- or low-concentration regions of $Ca^{2+}$, the peak of $Tb_3TCAS_2$ was observed. As the concentration of $Ca^{2+}$ increased, peak 1 appeared, and its height increased, reaching a maximum at the ratio of $Ca^{2+}$/TCAS = 0.5. In contrast, when the ratio of $Ca^{2+}$/TCAS was fixed at 0.5 and the concentration of $Tb^{3+}$ was varied, the peak of TCAS was observed at zero or low concentrations of $Tb^{3+}$ (Fig. 5). As the concentration of $Tb^{3+}$ increased, the height of peak 1 reached a maximum at $Tb^{3+}$/TCAS = 1.5.

These results suggest that the stoichiometry of the Ca–Tb–TCAS complex for peak 1 was Ca : Tb : TCAS = 0.5 : 1.5 : 1.0, implying the formation of the $Ca_1Tb_3TCAS_2$ complex. To confirm the formation of $Ca_1Tb_3TCAS_2$, ESI mass spectrometry was also performed at pH 6.0, adjusted with $NH_3$ solution, and $CH_3CN$ was added to the sample solution to facilitate the ionization process (Fig. 6 and S2†). The mass spectra exhibited intense peaks at $m/z$ 454.461738, which could be assigned to $[Ca^{2+} + 3Tb^{3+} + 2tcas^{8-} + 2Na^+ + 2OH^- + NH_3 + CH_3CN]^{5-}$ ($m/z$ 454.4581). All assignment is included in Fig. S2,† and other products with different metal ratios of Ca–Tb–TCAS complexes were not detected.

In previous studies, the results of ESI mass spectrometry showed many adducts in the metal complexes using TCAS ligand.[7,9–11] In our case, the adducts of $CH_3CN$ and $NH_3$ presenting as guest molecules in the TCAS ligand of the Ca–Tb–TCAS complexes is suggested,[13] and there is also the possibility for a coordinated $NH_3$ molecule with the latter because the Tb center of the Ca–Tb–TCAS complexes contains two coordinated water molecules (the details of this result will be discussed later,

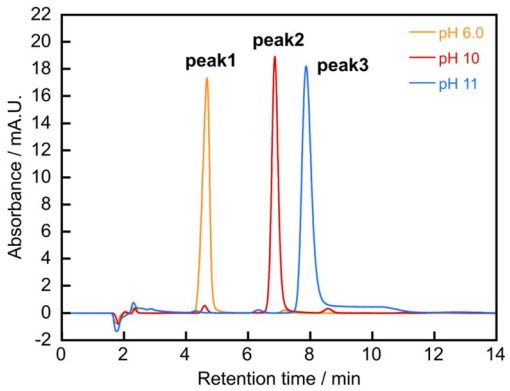


Fig. 3 Chromatograms of Ca–Tb–TCAS systems at different pH conditions. pH 6.0 condition: $[Ca^{2+}] = 10$ μM, $[Tb^{3+}] = 30$ μM, [TCAS] = 20 μM, [MES] = 20 mM, pH 6.0, $t = 24$ h, 60 °C; pH 10 condition: $[Ca^{2+}] = [Tb^{3+}] = [TCAS] = 20$ μM, [CAPS] = 20 mM, pH 10, $t = 24$ h, 60 °C; pH 11 condition: $[Ca^{2+}] = 30$ μM, $[Tb^{3+}] = 10$ μM, [TCAS] = 20 μM, pH 11 (adjusted with $NH_3$), $t = 1$ h, 60 °C.

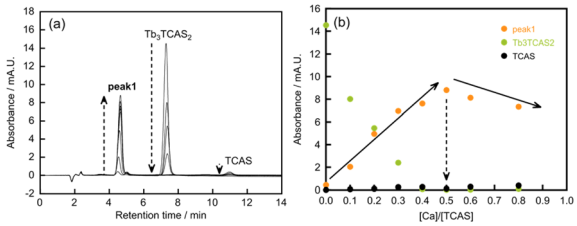


Fig. 4 (a) Chromatograms of the molar ratio method and (b) molar ratio curves between $[Ca^{2+}]$ and [TCAS] for the Ca–Tb–TCAS system at pH 6.0. $[Ca^{2+}] = 0-16$ μM, $[Tb^{3+}] = 30$ μM, [TCAS] = 20 μM, [MES] = 20 mM, pH 6.0, $\lambda = 316$ nm, $t = 24$ h, 60 °C.

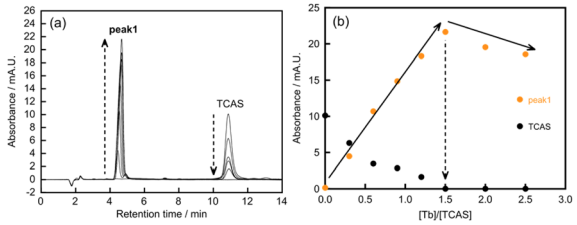


Fig. 5 (a) Chromatograms of the molar ratio method and (b) molar ratio curves between $[Tb^{3+}]$ and [TCAS] for the Ca–Tb–TCAS system at pH 6.0. $[Ca^{2+}] = 20$ μM, $[Tb^{3+}] = 0-0.10$ mM, [TCAS] = 40 μM, [MES] = 20 mM, pH 6.0, $\lambda = 316$ nm, $t = 24$ h, 60 °C.

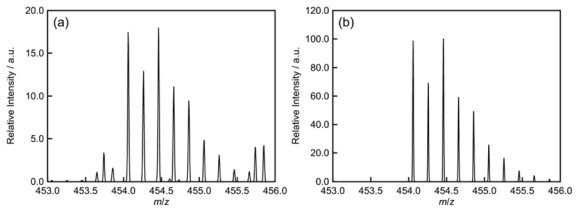


Fig. 6 ESI mass spectra of the Ca–Tb–TCAS system at pH 6.0. (a) Observed isotopic distribution at $m/z$ 454.461738 under the following conditions: $[Ca^{2+}] = 10$ μM, $[Tb^{3+}] = 30$ μM, [TCAS] = 20 μM, pH 6.0 (adjusted with $NH_3$), $t = 24$ h, 60 °C. (b) Calculated isotopic distribution for $[Ca^{2+} + 3Tb^{3+} + 2tcas^{8-} + 2Na^+ + 2OH^- + NH_3 + CH_3CN]^{5-}$ at $m/z$ $454.4581^{8-}$.

and see Table 1). Moreover, for other compounds with $O^{2-}$ and $H^+$, we assigned these compounds as consisting of $H_2O$ or $OH^-$. Thus, the $Ca_1Tb_3TCAS_2$ complex can be selectively formed at pH 6.0.

At pH 10, the molar ratio method at a fixed ratio of $Tb^{3+}$/TCAS = 1.0 with varying concentrations of $Ca^{2+}$ showed that the height of peak 2 reached a maximum at $Ca^{2+}$/TCAS = 1.0 (Fig. S3†). However, when the ratio of $Ca^{2+}$/TCAS was fixed at 1.0, and the concentration of $Tb^{3+}$ was varied, the height of peak 2 reached a maximum at $Tb^{3+}$/TCAS = 1.0 (Fig. S4†). These observations indicate that the stoichiometry of the complex is $Ca_iTb_iTCAS_i$ (*i*: natural number). Additionally, the ESI mass spectra of the sample solution at pH 10, which was adjusted with $NH_3$ solution and contained $CH_3CN$, showed intense peaks at *m*/*z* 708.782527, corresponding to the components of $[2Ca^{2+} + 2Tb^{3+} + 2tcas^{8-} + Na^+ + 2H^+ + 3H_2O + 2NH_3]^{3-}$ (*m*/*z* 708.7946) and other assignments, as shown in Fig. S5.† These results indicate that the stoichiometry of the Ca–Tb–TCAS system at pH 10 was $Ca_2Tb_2TCAS_2$.

At pH 11, the molar ratio plot of peak 3 showed a maximum at $Ca^{2+}$/TCAS = 1.5 when the $Tb^{3+}$/TCAS ratio was fixed at 0.5 (Fig. S6†). Furthermore, a maximum of peak 3 appeared at $Tb^{3+}$/TCAS = 0.5 when the $Ca^{2+}$/TCAS ratio was fixed at 1.5 (Fig. S7†). These results suggest that the $Ca_3Tb_1TCAS_2$ complex is primarily formed at pH 11; however, peaks of unwanted impurities, such as $Ca_2Tb_2TCAS_2$ and TCAS, were also observed. Therefore, a more suitable condition for the selective synthesis of the $Ca_3Tb_1TCAS_2$ complex was necessary.

Considering the success in enhancing the selectivity by adding TBABr during the synthesis of the Ln–Ln′–TCAS heterotrinuclear complex,[7b] we added tetrabutylammonium ($TBA^+$) bromide (TBABr) salt to the mixture of $Ca^{2+}$, $Tb^{3+}$, and TCAS to enhance the selectivity. Upon the addition of ≥0.2 M TBABr, the proportion of $Ca_3Tb_1TCAS_2$ increased, and that of $Ca_2Tb_2TCAS_2$ significantly decreased (Fig. S8†). The molar ratio method under the conditions of 0.2 M TBABr and pH 11 resulted in maxima at $Ca^{2+}$/TCAS = 1.5 (Fig. S9†) and at $Tb^{3+}$/TCAS = 0.5 (Fig. S10†). The effect of TBABr salt on the reaction is currently unclear and is still under investigation. We briefly described the effect of the TBABr salt as a hypothesis based on our previous findings.[7b] The presence of TBABr or $TBA^+$ affects the rate constant of the complexation reaction during the formation of a sandwich structure, leading to a decrease in the rate of the reaction step:

$$2Ln_1TCAS_1 \rightarrow Ln_2TCAS_2 \quad (1)$$

In the Ca–Tb–TCAS system, three reactions are involved in forming the 2 : 2 complexes, as shown below:

$$2Tb_1TCAS_1 \rightarrow Tb_2TCAS_2 \quad (1')$$

$$2Ca_1TCAS_1 \rightarrow Ca_2TCAS_2 \quad (2)$$

$$Tb_1TCAS_1 + Ca_1TCAS_1 \rightarrow Ca_1Tb_1TCAS_2 \quad (3)$$

We assume that the presence of TBABr or $TBA^+$ selectively decreases the reaction rate of eqn (1′). The ESI-MS analysis of the sample solution of the Ca–Tb–TCAS system, which was adjusted to pH 11 with $NH_3$ solution and contained $CH_3CN$, exhibited intense peaks at *m*/*z* 382.670041 and 382.8715772. This isotopic distribution corresponds to the components of $[3Ca^{2+} + Tb^{3+} + 2tcas^{8-} + H^+ + H_2O]^{5-}$ (*m*/*z* 382.6698) and $[3Ca^{2+} + Tb^{3+} + 2tcas^{8-} + 2H^+ + H_2O]^{5-}$ (*m*/*z* 382.8714), confirming the formation of the $Ca_3Tb_1TCAS_2$ complex at pH 11. Additionally, other signals and their assignments are shown in Fig. S11.†

We attempted to reveal the structure of these Ca–Tb–TCAS complexes. Despite some crystallization experiments, the single crystal suitable for X-ray diffraction analysis has not yet been obtained and is in progress. We preliminarily investigated isolation of a solid sample of the Ca–Tb–TCAS complexes as a salt with hexadecyltrimethylammonium ion ($CTMA^+$). We successfully obtained precipitates produced by the mixing of the Ca–Tb–TCAS complexes and $CTMA^+$.

In the mixture of the $Ca_1Tb_3TCAS_2$ complex and the $CTMA^+$ system, the CHN elemental analysis indicated that the composition of the salt was $CTMA_6Ca_1Tb_3TCAS_2(H_2O)_{10}Cl_1$. This result was consistent with the salt for the $Tb_3TCAS_2$ complex with quaternary ammonium ions in the previous study, for example, $CTMA_7Tb_3TCAS_2(H_2O)_{10}$.[16b] The other two complexes, $Ca_2Tb_2TCAS_2$ and $Ca_3Tb_1TCAS_2$, also showed similar compositions: $CTMA_{10}Ca_2Tb_2TCAS_2(H_2O)_{18}(NO_3)_3$ and $CTMA_{10}Ca_3Tb_1TCAS_2(H_2O)_{20}Cl_3$. These CTMA–Ca–Tb–TCAS salts contained $H_2O$ molecules as coordinated water (see Table 1) and crystal solvent, and the coprecipitation of CTMACl or $CTMANO_3$ salts was suggested due to the experimental conditions (addition of a small excess amount of CTMACl and cooling before filtration).

By simply mixing the components ($Ca^{2+}$, $Tb^{3+}$, and TCAS) at an appropriate ratio and appropriate pH (6.0, 10, and 11), selective formation of the $Ca_1Tb_3TCAS_2$, $Ca_2Tb_2TCAS_2$, and $Ca_3Tb_1TCAS_2$ complexes can be achieved using the thermodynamic strategy. The number of $Tb^{3+}$ in the Ca–Tb–TCAS complexes decreased at high pH, which may be attributed to the fact that $Tb^{3+}$ is more susceptible to hydrolysis compared to $Ca^{2+}$. This phenomenon is influenced by the valence of the metal ions.

The results of the present work show that the ratio of $Tb^{3+}$ and $Ca^{2+}$ ($Ca_1Tb_3$, $Ca_2Tb_2$, and $Ca_3Tb_1$) could be completely controlled by pH conditions despite their properties of chemical similarity. These systems enabled selective synthesis of heteronuclear complexes without the need for precise design or modification of the ligand. In addition, this observation is remarkably unique when compared to previous studies in which TCAS or TCA was used as a ligand containing a M–Ln core, and the chemical properties of M ($Ag^+$, $Cd^{2+}$, $Mn^{2+}$, $Zn^{2+}$) and Ln ($Tb^{3+}$, $Yb^{3+}$, $Nd^{3+}$, $Gd^{3+}$, $Dy^{3+}$, $Ho^{3+}$) are significantly different.[11b–d,14]

We assume that the Ca–Tb–TCAS complexes possess a double-cone structure in which the tetrametal core is sandwiched by two conical TCAS anions, as exemplified by $Ln_3TCAS_2$ and $Ln_4TCA_2$.[9,15] First, $Ca_1Tb_3TCAS_2$ can also be formed by mixing $Ca^{2+}$ and $Tb_3TCAS_2$ complex in the kinetic strategy (*vide infra*), suggesting that $Ca_1Tb_3TCAS_2$ adopts the double-cone structure. Second, the luminescence properties as well as the number of coordinated water molecules of the $Ca_2Tb_2TCAS_2$

and $Ca_3Tb_1TCAS_2$ complexes are very similar to those of $Ln_3$-$TCAS_2$ and $Ca_1Tb_3TCAS_2$, indicating the structural similarity among these complexes. Third, the chromatographic behavior of those complexes is very similar. The number of coordination bonds connecting the metal core and TCAS in the Ca–Tb–TCAS complexes is larger than that in the $Ln_3TCAS_2$ complex. Consequently, the kinetic stability of the heterotetranuclear Ca–Tb–TCAS complexes is expected to be greater than that of the $Tb_3TCAS_2$ complex.

### Time dependence of the self-assembly of the heterotetranuclear Ca–Tb–TCAS complexes

The self-assembly of the heterotetranuclear Ca–Tb–TCAS complexes was measured as a function of time under specific ratios of the components ($Ca^{2+}$, $Tb^{3+}$, and TCAS) at optimum pH (Fig. 7). At pH 6.0, peak 1 ($Ca_1Tb_3TCAS_2$) immediately appeared upon mixing the components, and reached a plateau after 120 min (Fig. 7(a)). The byproducts ($Tb_1TCAS_1$, $Tb_3TCAS_2$, and $Ca_2Tb_2TCAS_2$) decreased and eventually disappeared at 120 min, indicating the formation of a single $Ca_1Tb_3TCAS_2$ complex. There was an appearance by peak 2 ($Ca_2Tb_2TCAS_2$), which reached a plateau at 240 min, while the peaks of the byproducts $Ca_1Tb_3TCAS_2$ and $Ca_3Tb_1TCAS_2$ disappeared at pH 10 (Fig. 7(b)), indicating the formation of a single $Ca_2Tb_2TCAS_2$ complex. In the absence of TBABr at pH 11, not only peak 3 ($Ca_3Tb_1TCAS_2$) but also significant amounts of unwanted peak 2 $Ca_2Tb_2TCAS_2$ (approximately 25%) and TCAS appeared and persisted (Fig. S12†). In the presence of TBABr at pH 11, peak 2 and TCAS were substantially suppressed, and peak 3 was predominant for 150 min (Fig. 7(c)).

The time scale of the formation of each Ca–Tb–TCAS complex should be governed by a rate-determining step (RDS), which is different among the ternary complexes. For example, in Fig. 7(a), the increasing rate of peak 1 and decreasing rate of $Tb_3TCAS_2$ were the same, implying that the RDS is:

$$Ca^{2+} + Tb_3TCAS_2 \rightarrow Ca_1Tb_3TCAS_2 \quad (4)$$

In the case of Fig. 7(b), steps performed to change the composition of the tetrametal core should control the rate of formation of peak 2. Fig. 7(c) shows that the rate of formation of peak 3 and that of a decrease in TCAS are roughly the same, suggesting the presence of a key intermediate that does not significantly accumulate.

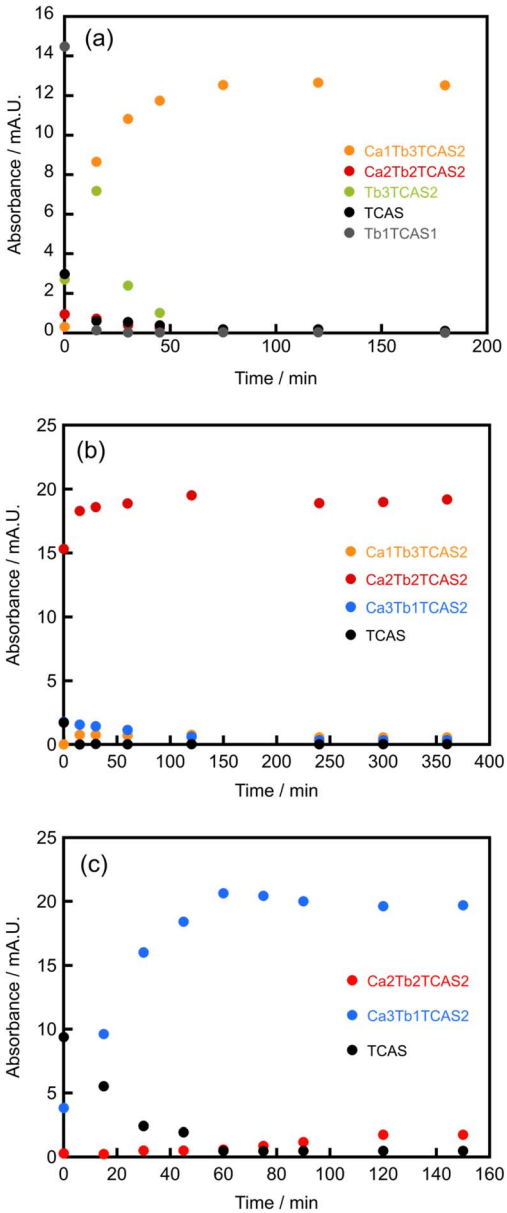


Fig. 7 Time dependence of the height of the HPLC peaks of the Ca–Tb–TCAS complexes during self-assembly. (a) $[Ca^{2+}]$ = 0.10 mM, $[Tb^{3+}]$ = 0.30 mM, [TCAS] = 0.20 mM, [MES] = 40 mM, pH 6.0, 60 °C. (b) $[Ca^{2+}]$ = 2.0 mM, $[Tb^{3+}]$ = 2.0 mM, [TCAS] = 2.0 mM, pH 10 (adjusted with $NH_3$), 60 °C. (c) $[Ca^{2+}]$ = 0.15 mM, $[Tb^{3+}]$ = 50 μM, [TCAS] = 0.10 mM, [TBABr] = 0.20 M, pH 11 (adjusted with $NH_3$), 60 °C.

### Synthesis of a heterotetranuclear Ca–Tb–TCAS complex using the kinetic strategy

Considering eqn (4), we prepared $Ca_1Tb_3TCAS_2$ by introducing $Ca^{2+}$ into $Tb_3TCAS_2$. One equivalent of $Ca^{2+}$ was added to a solution containing $Tb_3TCAS_2$ obtained by a previously reported method,[15] and the self-assembly process of the complexation was monitored. The peak of $Tb_3TCAS_2$ was dominant immediately after the addition of $Ca^{2+}$ (Fig. 8). Subsequently, the peak of $Tb_3TCAS_2$ decreased; however, peak 1 ($Ca_1Tb_3TCAS_2$) emerged and increased. Furthermore, peak 1 reached a plateau at 240 min, and the peak of $Tb_3TCAS_2$ disappeared. Thus, mere mixing of the $Tb_3TCAS_2$ complex and $Ca^{2+}$ afforded $Ca_1Tb_3TCAS_2$, which formed due to the kinetic stability of $Tb_3TCAS_2$; thus, this approach can be classified as a kinetic strategy. The times for reaching the plateau were not the same (120 min in Fig. 7(a) and 240 min in Fig. 8), which can be attributed to the difference in the pH conditions.

### Luminescence properties of the heterotetranuclear Ca–Tb–TCAS complexes

The excitation spectra of the three heterotetranuclear Ca–Tb–TCAS complexes ($Ca_xTb_{4-x}TCAS_2$, $x$ = 1–3) exhibited a broad

peak, attributed to the π–π* transition of ligand-centered absorption (Fig. 9(a)). The wavelengths of the excitation peaks were disparate, with values of 314 nm for $Ca_1Tb_3TCAS_2$, 320 nm for $Ca_2Tb_2TCAS_2$, and 326 nm for $Ca_3Tb_1TCAS_2$. The wavelength of the peaks depended on the charge of the metal core; that is, the smaller the number of the charges of the tetrametal core (*i.e.*, +11 for $Ca_1Tb_3$, +10 for $Ca_2Tb_2$, and +9 for $Ca_3Tb_1$), the longer the excitation wavelength. The emission spectra of the complexes $Ca_xTb_{4-x}TCAS_2$ ($x$ = 1–3) exhibited sharp emission bands, corresponding to Tb-centered luminescence ($^5D_4 \rightarrow {}^7F_J$, $J$ = 6–3). The ligand-centered absorption and the Tb-centered luminescence suggest that all heterotetranuclear Ca–Tb–TCAS complexes ($Ca_xTb_{4-x}TCAS_2$, $x$ = 1–3) exhibited luminescence through energy transfer from TCAS to $Tb^{3+}$.

In the fine structure of Tb-centered luminescence ($^5D_4 \rightarrow {}^7F_J$, $J$ = 5, 4), the shapes of the bands for the $Ca_1Tb_3TCAS_2$, $Ca_2Tb_2TCAS_2$, and $Ca_3Tb_1TCAS_2$ complexes were not identical (Fig. 9(b and c)). Notably, the luminescence spectra of the $Ca_3Tb_1TCAS_2$ complex exhibited significantly different shapes compared to those of the $Ca_1Tb_3TCAS_2$ and $Ca_2Tb_2TCAS_2$ complexes. In general, the fine structure of the Tb-centered luminescence depends on the coordination environment of the $Tb^{3+}$ center. Assuming a sandwich-type structure for all Ca–Tb–TCAS complexes, the difference in the coordination environment of the $Tb^{3+}$ center can be understood by the electron density of $\mu_2$-O, a phenol oxygen atom of TCAS ($O_{TCAS}$), bridging two metal centers according to Ca-$O_{TCAS}$-Ca, Ca-$O_{TCAS}$-Tb, and Tb-$O_{TCAS}$-Tb (Fig. 10).

The electron density of $\mu_2$-O decreases in the following order: Ca-$O_{TCAS}$-Ca > Ca-$O_{TCAS}$-Tb > Tb-$O_{TCAS}$-Tb. Considering this order, the $Tb^{3+}$ center in the $Ca_3Tb_1TCAS_2$ is coordinated by two $\mu_2$-O (Ca-$O_{TCAS}$-Tb) with an intermediate electron density. For $Ca_1Tb_3TCAS_2$, two of the $Tb^{3+}$ centers are coordinated by $\mu_2$-O of Ca-$O_{TCAS}$-Tb, but one is coordinated by the most electron-deficient $\mu_2$-O (Tb-$O_{TCAS}$-Tb). Therefore, it is likely that the difference between the fine structures of the Tb-centered luminescence of the $Ca_1Tb_3TCAS_2$ and $Ca_3Tb_1TCAS_2$ complexes originated from the presence or the absence of the Tb-$O_{TCAS}$-Tb type of $\mu_2$-O.

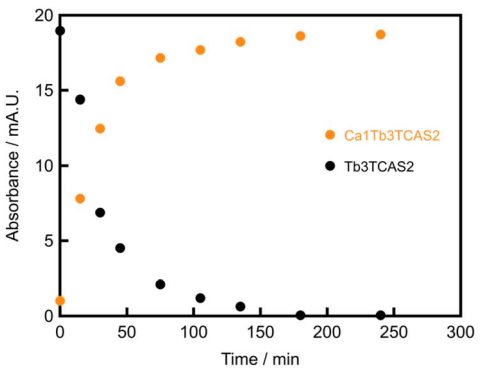


Fig. 8 Time dependence of the height of the HPLC peaks of the $Ca_1Tb_3TCAS_2$ complex in the mixture of the $Tb_3TCAS_2$ complex and $Ca^{2+}$. [$Ca^{2+}$] = 0.10 mM, [$Tb_3TCAS_2$] = 0.10 mM, pH 10 (adjusted with $NH_3$), 60 °C.

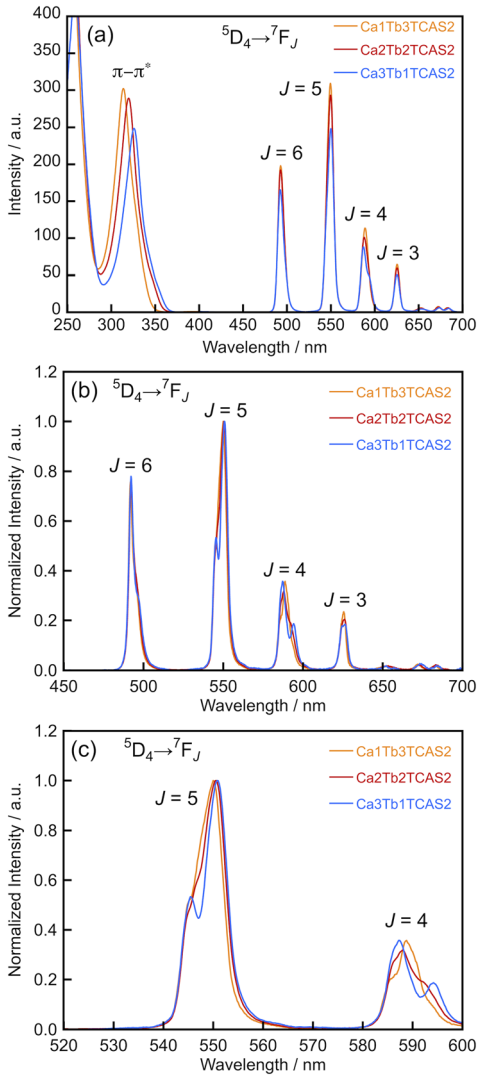


Fig. 9 (a) Excitation and emission spectra and (b and c) the fine-structure of Tb-centered luminescence for the Ca–Tb–TCAS systems. The $Ca_1Tb_3TCAS_2$ system: [$Ca_1Tb_3TCAS_2$] = 1.0 μM, [CAPS] = 10 mM, pH 10, $\lambda_{ex}$ = 314 nm, $\lambda_{em}$ = 550 nm, $t$ = 24 h, 60 °C; the $Ca_2Tb_2TCAS_2$ system: [$Ca_2Tb_2TCAS_2$] = 1.0 μM, [CAPS] = 10 mM, pH 10, $\lambda_{ex}$ = 320 nm, $\lambda_{em}$ = 550 nm, $t$ = 24 h, 60 °C; and the $Ca_3Tb_1TCAS_2$ system: [$Ca_3Tb_1TCAS_2$] = 1.0 μM, [TBABr] = 20 mM, pH 10.5 (adjusted with $NH_3$), $\lambda_{ex}$ = 326 nm, $\lambda_{em}$ = 550 nm, $t$ = 1 h, 60 °C. (a) The width of the excitation and emission slits was 5 nm. (b and c) The width of the excitation slit was 20 nm, and the width of the emission slit was 1 nm. Normalized at 550 nm.

For $Ca_2Tb_2TCAS_2$, there are two possible configurations: a diagonal arrangement (Ca–Tb–Ca–Tb disposition) or an arrangement adjacent to an identical metal center (Ca–Ca–Tb–Tb disposition) (Fig. 10). These configurations represent distinct types of $\mu_2$-O: the Ca–Tb–Ca–Tb disposition has only one type of $\mu_2$-O, that is, Ca–$O_{TCAS}$-Tb; however, the Ca–Ca–Tb–Tb disposition has two types of $\mu_2$-O, that is, Ca–$O_{TCAS}$–Tb and Tb–$O_{TCAS}$–Tb. Because the shape of the luminescence bands of $Ca_2Tb_2TCAS_2$ is similar to that of $Ca_1Tb_3TCAS_2$ with Tb–$O_{TCAS}$–Tb, the arrangement of the tetrametal core in $Ca_2Tb_2TCAS_2$ is possibly Ca–Ca–Tb–Tb.

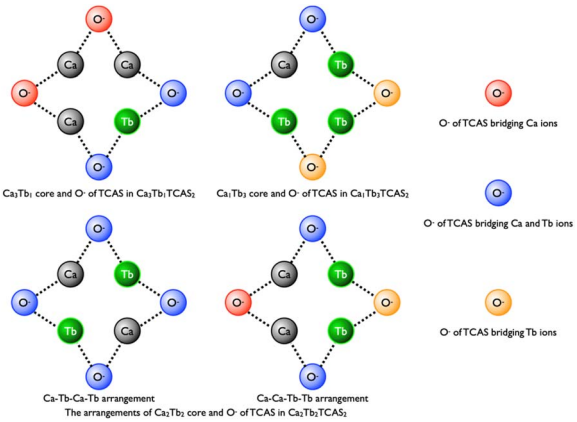


Fig. 10 Arrangements of the Ca–Tb core and three types of phenol oxygen atom of TCAS in the heterotetranuclear complexes.

This hypothesis is reasonable by considering the coordination bond length of M–$O_{TCAS}$ or M–S, which should be different among M = $Ca^{2+}$ and $Tb^{3+}$. The Ca–Ca–Tb–Tb disposition is more tolerant than the Ca–Tb–Ca–Tb disposition toward sandwiching the metal core while maintaining the optimal M–$O_{TCAS}$ and M–S length. Consequently, two conical TCAS ligands were not in parallel alignment, but rather, were aligned in a slightly tilted manner. In fact, examples of such M–M–Ln–Ln arrangements in M–Ln–thiacalixarene systems have been previously reported;[11b–d,14a] however, no arrangements of M–Ln–M–Ln have been reported.

Table 1 summarizes the photophysical properties of the heterotetranuclear Ca–Tb–TCAS complexes ($Ca_xTb_{4-x}TCAS_2$, $x$ = 1–3) and the previously reported $Tb_3TCAS_2$ complex. The Tb-centered luminescence lifetime for the three heterotetranuclear complexes was long, with equal values of approximately 1.2 ms. The number of coordinated water molecules was estimated to be two for each heterotetranuclear complex by Horrocks' equation[17] and the luminescence lifetimes in $H_2O$ and $D_2O$. The quantum yield of the three heterotetranuclear complexes was 0.11–0.14. The luminescence properties of the heterotetranuclear complexes were as high as those of the previously reported homotrinuclear $Tb_3TCAS_2$ complex,[16] indicating that they possess a similar sandwich-type structure and octa-coordination environment of the $Tb^{3+}$ center by two O, S, O donor sets from two TCAS ligands and two oxygen atoms from water.[9]

Table 1 Quantum yield ($\phi$)[a], luminescence lifetime ($\tau$)[b], and the number of coordinating water molecules per $Tb^{3+}$ center ($q$)[c] for the Ca–Tb–TCAS and $Tb_3TCAS_2$ complexes

| | $\phi$/— | $\tau_H$/ms | $\tau_D$/ms | $q$ |
|---|---|---|---|---|
| $Ca_3Tb_1TCAS_2$ | 0.11 | 1.19 | 3.50 | 2.3 |
| $Ca_2Tb_2TCAS_2$ | 0.13 | 1.19 | 2.81 | 2.1 |
| $Ca_1Tb_3TCAS_2$ | 0.14 | 1.22 | 2.90 | 2.0 |
| $Tb_3TCAS_2$[d] | 0.14 | 1.12 | 3.22 | 2.4 |

[a] [complex] = 0.25 μM, [CAPS] = 10 mM, pH 10, $\lambda_{ex}$ = 314 nm for $Ca_1Tb_3TCAS_2$, 320 nm for $Ca_2Tb_2TCAS_2$, 326 nm for $Ca_3Tb_1TCAS_2$, $t$ = 24 h for $Ca_1Tb_3TCAS_2$ and $Ca_2Tb_2TCAS_2$, 1 h for $Ca_3Tb_1TCAS_2$. [b] For the decay curves, see Fig. S13–15 in ESI. Subscripts H and D for $\tau$ denote $H_2O$ and $D_2O$ solvents, respectively. [c] Estimated by Horrocks' equation. $q = 4.19(\tau_H^{-1} - \tau_D^{-1})$. [d] See ref. 16.

## Thermodynamic and kinetic strategies for other metal ions to form heterotetranuclear M–Tb–TCAS complexes

Inspired by the success of the selective preparation of three types of Ca–Tb–TCAS heterotetranuclear complexes using the thermodynamic strategy, and the preparation of $Ca_1Tb_3TCAS_2$ using the kinetic strategy, we extended the strategy to other alkaline earth and transition metal ions (M) (Fig. S16†). For example, the chromatograms of the reaction mixture in the thermodynamic strategy (M : Tb : TCAS = 1 : 3 : 2, pH 6.0 and M : Tb : TCAS = 2 : 2 : 2, pH 10) showed a single peak in the presence of TCAS and $Tb^{3+}$ with M = $Sr^{2+}$ at the retention time ($t_R$ = 4.53 min for Sr : Tb : TCAS = 1 : 3 : 2 at pH 6.0, 6.56 min for M:Tb:TCAS = 2 : 2 : 2 at pH 10), which was similar to that for one of the Ca–Tb–TCAS complexes ($t_R$ = 4.67 min for $Ca_1Tb_3TCAS_2$, 6.86 min for $Ca_2Tb_2TCAS_2$). In contrast, the chromatograms of the transition metal systems (M = $Ti^{3+}$, $Mn^{2+}$, $Fe^{2+}$, $Co^{2+}$, $Ni^{2+}$, $Cu^{2+}$, $Zn^{2+}$) showed several peaks corresponding to various M–Tb–TCAS and Tb–TCAS complexes. This may be caused by many factors, including the affinity for the TCAS ligand, complexation kinetics, and the tendency towards hydrolysis of transition metal ions other than $Ca^{2+}$. Hence, the optimum conditions for the formation of heterotetranuclear M–Tb–TCAS complexes should be different from those for the formation of Ca–Tb–TCAS.

In contrast, the kinetic strategy using the reaction between $Tb_3TCAS_2$ and metal ions (M) resulted in a single peak in all systems, and $M_1Tb_3TCAS_2$ complexes (M = $Sr^{2+}$, $Mn^{2+}$, $Fe^{2+}$, $Co^{2+}$, $Ni^{2+}$, $Cu^{2+}$, $Zn^{2+}$) were successfully formed. The peak of the Sr–$Tb_3TCAS_2$ system appeared at $t_R$ = 4.35 min, which is similar to that of the $Ca_1Tb_3TCAS_2$ complex ($t_R$ = 4.67 min). For the transition metal-$Tb_3TCAS_2$ systems, a single peak appeared at $t_R$ = 5.22–5.35 min, which is different than that of the $Ca_1Tb_3TCAS_2$ complex. This may have been caused by the difference in the charge of the M and/or in the deprotonation of the coordinating water to M. Thus, the kinetic strategy can be applied not only to $Ca^{2+}$, but also to various metal ions.

We further investigated the ESI mass spectrometry for the mixture of M and the $Tb_3TCAS_2$ solution to confirm the formation of the $M_1Tb_3TCAS_2$ complex (M = $Sr^{2+}$, $Mn^{2+}$, $Fe^{2+}$, $Co^{2+}$, $Ni^{2+}$, $Cu^{2+}$, $Zn^{2+}$) (Fig. S17–23†). For example, the mixture of $Sr^{2+}$ and $Tb_3TCAS_2$ solution showed isotopic distribution at $m/z$ 443.24429, which could be assigned to $[Sr^{2+} + 3Tb^{3+} + 2tcas^{8-} + 2H_2O]^{5-}$ ($m/z$ 443.2449) (Fig. S17†). This result indicates the formation of the $Sr_1Tb_3TCAS_2$ complex. The others also showed mass spectra corresponding to $[M^{2+} + 3Tb^{3+} + 2tcas^{8-} + 2H_2O]^{5-}$ (M = $Sr^{2+}$, $Mn^{2+}$, $Fe^{2+}$, $Co^{2+}$, $Ni^{2+}$, $Zn^{2+}$) and $[Cu^{2+} + 3Tb^{3+} + 2tcas^{8-} + H_2O]^{5-}$. These ESI-MS measurement results are consistent with the above HPLC measurements, implying that the formation of the $M_1Tb_3TCAS_2$ complex could be possible by the mixture of M and $Tb_3TCAS_2$ solution at pH 6.0. Moreover, the mixture of M and $Tb_3TCAS_2$ emitted Tb-

centered luminescence due to energy transfer from TCAS ligand, but the intensity at 550 nm was different depending on the type of metal ion (M) (Fig. S24†).

In the case of M = $Sr^{2+}$ or $Zn^{2+}$, the intensity at 550 nm was the same as that of the $Tb_3TCAS_2$ complex. In contrast, in the case of M = $Mn^{2+}$, $Fe^{2+}$, $Co^{2+}$, $Ni^{2+}$, or $Cu^{2+}$, the Tb-centered luminescence was diminished, indicating paramagnetic quenching. According to the above findings, the mixture of M and $Tb_3TCAS_2$ produces $M_1Tb_3TCAS_2$ complexes (M = $Sr^{2+}$, $Mn^{2+}$, $Fe^{2+}$, $Co^{2+}$, $Ni^{2+}$, $Cu^{2+}$, $Zn^{2+}$).

## Conclusions

Herein, we presented a facile method to selectively prepare three luminescent heterotetranuclear complexes ($Ca_xTb_{4-x}TCAS_2$, $x$ = 1–3), in which heterometal cores are arranged in a square form. In the thermodynamic strategy, three complexes ($Ca_xTb_{4-x}TCAS_2$, $x$ = 1–3) were formed by simply mixing Ca, Tb, and TCAS at an appropriate proportion with an optimized pH. The selectivity of the formation of heterotetranuclear complexes seemingly depends upon the fact that the tendency of $Tb^{3+}$ to hydrolyze is greater than that of $Ca^{2+}$ (Fig. 11). This result suggests that the difference in the susceptibility to hydrolysis between heterometal ions is a useful factor to control the heterometal core.

Moreover, this method can be applied not only to the TCAS ligand but also to many other ligands. In the kinetic strategy, $Ca_1Tb_3TCAS_2$ was afforded by simple addition of $Ca^{2+}$ to $Tb_3TCAS_2$ in solution (Fig. 11). All heterotetranuclear complexes ($Ca_xTb_{4-x}TCAS_2$, $x$ = 1–3) exhibited Tb-centered luminescence by an energy-transfer mechanism with nearly the same lifetime and quantum yield. However, the heterotetranuclear complex is kinetically more stable than the $Ln_3TCAS_2$ complex because of the multi-coordination bond by the tetranuclear core. Finally, we extended the strategies to the preparation of M–Tb–TCAS complexes (M = $Sr^{2+}$, $Mn^{2+}$, $Fe^{2+}$, $Co^{2+}$, $Ni^{2+}$, $Cu^{2+}$, $Zn^{2+}$). Because thiacalixarene ligands can form a metal complex with all $Ln^{3+}$ species[9] and various transition metal ions,[11d] the strategy may be applicable to other metal–lanthanide–TCAS complexes. Thus, the strategies mentioned in this study are promising, and will pave the way for the application of heterometal complexes in multimodal probes and multifunctional materials.

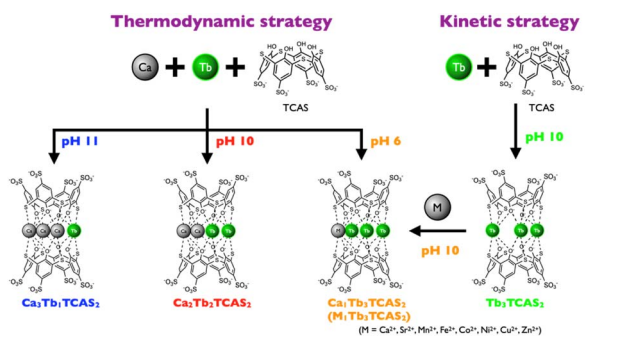


Fig. 11 Schematic of the formation of the heterotetranuclear Ca–Tb–TCAS complexes.

## Data availability

The data supporting this article have been included as part of the ESI.†

## Author contributions

Ryunosuke Karashimada: conceptualization, data curation, funding acquisition, investigation, project administration, resources, supervision, visualization, writing–original draft, writing–review and editing; Hironori Matsuoka: data curation, investigation, validation, visualization; Nobuhiko Iki: funding acquisition, project administration, resources, supervision, writing–review and editing.

## Conflicts of interest

There are no conflicts to declare.

## Acknowledgements

ESI-MS measurements were supported by Mr Hiroyuki Momma and Shunsuke Kayamori. This work was partly supported by JSPS KAKENHI (Grant Numbers 18K14248, 20K15308, and 23K04801).

## References

1 (*a*) F. Artizzu, F. Quochi, A. Serpe, E. Sessini and P. Deplano, *Inorg. Chem. Front.*, 2015, **2**, 213–222; (*b*) J.-R. Jiménez, B. Doistau, M. Poncet and C. Piguet, *Coord. Chem. Rev.*, 2021, **434**, 513750–513769; (*c*) X.-Z. Li, C.-B. Tian and Q.-F. Sun, *Chem. Rev.*, 2022, **122**, 6374–6458; (*d*) Z. Zhu and J. Tang, *Chem. Soc. Rev.*, 2022, **51**, 9469–9481; (*e*) Y. Peng, H. Kaemmerer and A. K. Powell, *Chem. Eur J.*, 2021, **27**, 15043–15065; (*f*) Q. Wang, S. H. Brooks, T. Liu and N. C. Tomson, *Chem. Commun.*, 2021, **57**, 2839–2853; (*g*) Z.-H. Pan, Z.-Z. Weng, X.-J. Kong, L.-S. Long and L.-S. Zheng, *Coord. Chem. Rev.*, 2022, **457**, 214419–214440.

2 (*a*) J.-C. G. Bünzli, *Chem. Rev.*, 2010, **110**, 2729–2755; (*b*) J.-C. G. Bünzli and S. V. Eliseeva, *J. Rare Earths*, 2010, **28**, 824–842; (*c*) S. V. Eliseeva and J.-C. G. Bünzli, *Chem. Soc. Rev.*, 2010, **39**, 189–227; (*d*) M. Sy, A. Nonat, N. Hildebrandt and L. J. Charbonnière, *Chem. Commun.*, 2016, **52**, 5080–5095.

3 (*a*) N. Iki, *Supramol. Chem.*, 2011, **23**, 160–168; (*b*) A. M. Nonat and L. J. Charbonnière, *Coord. Chem. Rev.*, 2020, **409**, 213192–213208.

4 (*a*) L. Aboshyan-Sorgho, H. Nozary, A. Aebischer, J.-C. G. Bünzli, P.-Y. Morgantini, K. R. Kittilstved, A. Hauser, S. V. Eliseeva, S. Petoud and C. Piguet, *J. Am. Chem. Soc.*, 2012, **134**, 12675–12684; (*b*) D. Zare, Y. Suffren, L. Guénée, S. V. Eliseeva, H. Nozary, L. Aboshyan-Sorgho, S. Petoud, A. Hauser and C. Piguet, *Dalton Trans.*, 2015, **44**, 2529–

2540; (*c*) D. Zare, Y. Suffren, H. Nozary, A. Hauser and C. Piguet, *Angew. Chem., Int. Ed.*, 2017, **56**, 14612–14617.

5 (*a*) F. Artizzu, F. Quochi, L. Marchiò, E. Sessini, M. Saba, A. Serpe, A. Mura, M. L. Mercuri, G. Bongiovanni and P. Deplano, *J. Phys. Chem. Lett.*, 2013, **4**, 3062–3066; (*b*) F. Artizzu, F. Quochi, L. Marchiò, R. F. Correia, M. Saba, A. Serpe, A. Mura, M. L. Mercuri, G. Bongiovanni and P. Deplano, *Chem. Eur J.*, 2014, **21**, 3882–3885; (*c*) F. Artizzu, F. Quochi, L. Marchiò, C. Figus, D. Loche, M. Atzori, V. Sarritzu, A. M. Kaczmarek, R. V. Deun, M. Saba, A. Serpe, A. Mura, M. L. Mercuri, G. Bongiovanni and P. Deplano, *Chem. Mater.*, 2015, **27**, 4082–4092; (*d*) F. Artizzu, A. Serpe, L. Marchiò, M. Saba, A. Mura, M. L. Mercuri, G. Bongiovanni, P. Deplano and F. Quochi, *J. Mater. Chem. C*, 2015, **3**, 11524–11530.

6 (*a*) N. Souri, P. Tian, C. Platas-Iglesias, K.-L. Wong, A. Nonat and L. J. Charbonnière, *J. Am. Chem. Soc.*, 2017, **139**, 1456–1459; (*b*) J. Salaam, L. Tabti, S. Bahamyirou, A. Lecointre, O. H. Alba, O. Jeannin, F. Camerel, S. Cianférani, E. Bentouhami, A. M. Nonat and L. J. Charbonnière, *Inorg. Chem.*, 2018, **57**, 6095–6106; (*c*) A. Nonat, S. Bahamyirou, A. Lecointre, F. Przybilla, Y. Mély, C. Platas-Iglesias, F. Camerel, O. Jeannin and L. J. Charbonnière, *J. Am. Chem. Soc.*, 2019, **141**, 1568–1576; (*d*) R. C. Knighton, L. K. Soro, T. Troadec, V. Mazan, A. M. Nonat, M. Elhabiri, N. Saffon-Merceron, S. Djenad, R. Tripier and L. J. Charbonnière, *Inorg. Chem.*, 2020, **59**, 10311–10327; (*e*) R. C. Knighton, L. K. Soro, A. Lecointre, G. Pilet, A. Fateeva, L. Pontille, L. Francés-Soriano, N. Hildebrandt and L. J. Charbonnière, *Chem. Commun.*, 2021, **57**, 53–56; (*f*) L. K. Soro, C. Charpentier, F. Przybilla, Y. Mély, A. M. Nonat and L. J. Charbonnière, *Chem. Eur J.*, 2021, **3**, 1037–1046; (*g*) R. C. Knighton, L. K. Soro, L. Francés-Soriano, A. Rodríguez-Rodríguez, G. Pilet, M. Lenertz, C. Platas-Iglesias, N. Hilderbrandt and L. J. Charbonnière, *Angew. Chem., Int. Ed.*, 2022, **61**, e202113114.

7 (*a*) R. Karashimada and N. Iki, *Chem. Commun.*, 2016, **52**, 3139–3142; (*b*) R. Karashimada, K. Musha and N. Iki, *Bunseki Kagaku*, 2022, **71**, 145–151.

8 N. Morohashi and N. Iki, *Handbook on the Physics and Chemistry of Rare Earths*, Elsevier, 2022, vol. 326, pp. 1–280.

9 N. Iki, T. Tanaka, S. Hiro-oka and K. Shinoda, *Eur. J. Inorg. Chem.*, 2016, 5020–5027.

10 (*a*) N. Iki, E. Boros, M. Nakamura, R. Baba and P. Caravan, *Inorg. Chem.*, 2016, **55**, 4000–4005; (*b*) N. Iki, S. Hiro-oka, M. Nakamura, T. Tanaka and H. Hoshino, *Eur. J. Inorg. Chem.*, 2012, 3541–3545; (*c*) N. Iki, S. Hiro-oka, T. Tanaka, C. Kabuto and H. Hoshino, *Inorg. Chem.*, 2012, **51**, 1648–1656.

11 (*a*) T. Tanaka, N. Iki, T. Kajiwara, M. Yamashita and H. Hoshino, *J. Inclusion Phenom. Macrocyclic Chem.*, 2009, **64**, 379–383; (*b*) N. Iki, M. Ohta, T. Horiuchi and H. Hoshino, *Chem. Asian J.*, 2008, **3**, 849–853; (*c*) N. Iki, M. Ohta, T. Tanaka, T. Horiuchi and H. Hoshino, *New J. Chem.*, 2009, **33**, 23–25; (*d*) N. Iki, T. Tanaka and H. Hoshino, *Inorg. Chim. Acta*, 2013, **397**, 42–47.

12 Y. Kang, L. Xu, J. Dong, Y. Huang, X. Yuan, R. Li, L. Chen, Z. Wang and X. Ji, *Coord. Chem. Rev.*, 2023, **481**, 215050–215068.

13 N. Iki, T. Fujimoto and S. Miyano, *Chem. Lett.*, 1998, **27**, 625–626.

14 (*a*) Y. Bi, Y. Li, W. Liao, H. Zhang and D. Li, *Inorg. Chem.*, 2008, **47**, 9733–9735; (*b*) K. Su, F. Jiang, J. Qian, M. Wu, K. Xiong, Y. Gai and M. Hong, *Inorg. Chem.*, 2013, **52**, 3780–3786.

15 A. Bilyk, J. W. Dunlop, R. O. Fuller, A. K. Hall, J. M. Harrowfield, M. W. Hosseini, G. A. Koutsantonis, I. W. Murray, B. W. Skelton, A. N. Sobolev, R. L. Stamps and A. H. White, *Eur. J. Inorg. Chem.*, 2010, 2127–2152.

16 (*a*) N. Shiraishi, R. Karashimada and N. Iki, *Bull. Chem. Soc. Jpn.*, 2019, **92**, 1847–1852; (*b*) N. Shiraishi, D. Iikura, R. Karashimada and N. Iki, *J. Lumin.*, 2024, **269**, 120521–120529.

17 W. D. H. Jr and D. R. Sundnick, *Acc. Chem. Res.*, 1981, **14**, 384–392.